Plasmonic Paper-Based Flexible SERS Biosensor for Highly Sensitive Detection of Lactic and Uric Acid

M. Verma, Tania K. Naqvi, Santosh K. Tripathi, Manish M. Kulkarni, N. Eswara Prasad, and Prabhat K. Dwivedi

***Abstract*— Selective detection and quantification of biomarkers related to human diseases are essential for preventive healthcare. Surface-enhanced Raman scattering (SERS) spectroscopy is a powerful analytical tool offering high sensitivity. However, the success of this promising analytical tool relies on the ability to effectively fabricate SERS substrate. Herein we have demonstrated a plasmonic paper-based flexible substrate (PPFS) for SERS sensing. In situ growth of silver nanostructures (AgNS) on the paper-based substrate was achieved by using a simple one-step silver mirror reaction (SMR). FESEM and TEM results depicts that the increasing silver ion content influences the morphology (growth of multifacets), as well as size of AgNS. Further, the PPFS substrate was tested with Rhodamine-6G (Rh-6G) dye and an attomole sensitivity with a LOD of 4.54×10^{-18} M was achieved. Further, two biomarkers, lactic acid (LA) and uric acid (UA) were detected on the PPFS substrate, with μM and pM sensitivity, having LOD values of 0.6×10^{-6} and 0.3×10^{-12} M respectively. Above detection levels for UA on PPFS is two orders better than reported values, whereas for LA it is comparable with reported substrates. Finally, UA, LA and their mixtures were tested on PPFS and results compared with commercial substrate. The performance of PPFS were found better in all cases, thus, multifaceted AgNS paper based PPFS offers the potential to be used as a biosensor for detection of various biomarkers from body fluids, responsible for the detection of the critical disease for preventive health care.**

***Index Terms*— Plasmonic nanostructures, flexible paper substrate, SERS, Rh-6G, uric and lactic acid.**

I. Introduction

HUMAN health has always been a prime concern for scientific society, thus current research focuses on the development of diagnostic (point-of-care) platforms for on-site investigation of biological fluids for preventive healthcare [1].

Manuscript received July 7, 2021; revised October 7, 2021; accepted October 26, 2021. Date of publication October 28, 2021; date of current version April 1, 2022. This work was supported by the Defence Materials and Stores Research and Development Establishment (DMSRDE), Kanpur, India, under Project TR/0569/CARS/126. *(Corresponding author: Prabhat K. Dwivedi.)*

M. Verma, Tania K. Naqvi, Manish M. Kulkarni, and Prabhat K. Dwivedi are with the Centre for Nanosciences, Indian Institute of Technology Kanpur, Kanpur 208016, India (e-mail: prabhatd@iitk.ac.in).

Santosh K. Tripathi and N. Eswara Prasad are with the Defence Materials and Stores Research and Development Establishment, Kanpur 208013, India.

This article has supplementary downloadable material available at https://doi.org/10.1109/TNB.2021.3124055, provided by the authors.

Digital Object Identifier 10.1109/TNB.2021.3124055

Blood which forms the main body fluid, possesses much vital information correlated to health issues [2]. Metabolism of muscle cells, and liver governs the production of lactic acid (LA) in the blood, which gets amassed intracellularly due to inadequate supply of oxygen to tissues for aerobic oxidation of glucose molecule [3], [4]. Thus, the amount of LA in the blood can be directly associated with the muscle tolerance factor generated during physical exercise [4]. High levels of LA in blood samples had been correlated to health concerns like hypoxia, diabetic ketoacidosis, and heart failure [4]. Any negligence in normalizing LA content in patient blood could result in mortality [4], [5]. Presently, clinical measurement of LA in blood requires sample collection and its enzyme-mediated electrochemical analysis [4], [5]. Moreover, the LA extraction from blood samples requires procedures avoiding the reduction of LA by RBCs, like ice preservation followed by immediate centrifugation of samples [4]–[6]. Therefore, continuous monitoring of LA in blood samples becomes difficult using prevalent techniques [6]–[9]. Thus, the use of real-time techniques becomes imperative for the determination of LA levels in the blood.

Similarly, another biomarker, uric acid (UA) is the final product of the metabolic breakdown of purine nucleotides is a component of human urine [10], [11]. UA has been identified as a biomarker for diseases like gout, renal, cardiovascular, and Pre-eclampsia when its concentration in urine crosses 7/6 mg/dL in men/women [12]–[17]. Thus, the detection of UA becomes significant for a healthy living of a person. Various techniques like, electrochemical, colorimetric enzymatic assays, liquid chromatography, and capillary electrophoresis have been reported for the determination of UA, with disadvantages like, low concentration, time-consuming, assay-based tests, expensive enzymes, sophisticated instrumentation [16]–[18]. Therefore, it becomes imperative to develop a rapid, inexpensive, routine-based diagnostic kits for timely detection of UA, to control hyperuricemia conditions for patient health [16]–[22].

Surface-enhanced Raman scattering (SERS) spectroscopy, a noninvasive technique prevalent for label-free fingerprint detection of analytes, with a wide variety of applications like immunoassays, medicine, biochemical sensing, and food safety could meet the changes [3], [4]. In SERS, mainly two mechanisms are responsible for the Raman intensity enhancement, electromagnetic (EM) and chemical (CM).

In SERS, nanostructure and the analyte interaction are vital, due to the gap-dependent electromagnetic enhancement mechanism. The existence and control of 'hot-spot' regions for signal enhancement, via interparticle coupling with electromagnetic fields, has received much attention [3], [4]. Thus, efforts to address the low stability of aggregated colloidal metallic NPs, and low-affinity analytes for metallic NPs for SERS is being eplored [3], [4]. In SERS coupling of electric field enables detection of weak Raman signals from analytes with high sensitivity converging to single-molecule tracing [1]–[4], [23]–[27]. SERS sensors utilize hot spot regions in terms of uniformity and density to exploit the localized surface plasmon resonance (LSPR) scattering from nanostructures [1]–[6]. Studies, like the determination of glucose, LA, pyruvate, urea using the Raman techniques have been well reported, with the inclusion of numerous components like albumin, triglyceride, glucose present in serum [1], [9]–[11]. Thus, SERS biosensors offer a wide applicability in the detection of nucleic acids, proteins, glucose, in-vivo tumors, etc.

To meet the above health challenges fabrication of efficient SERS sensors is much needed. Flexible SERS sensors offer high adsorption and diffusion of analyte molecules on the substrate to generate intense Raman signals through flexibility, porous nature, high specific surface area, portability, and biodegradability [18]. These flexible SERS sensors, like plastic polymers and papers offer superiority over traditionally hard substrates in terms of cost, and innovative fabrication technique, besides the ease of absorbent on 3D surfaces [28]. Flexible sensors offer swab for stick and peel-off applications for collecting biological fluids by dipping, rubbing, lateral/vertical flow devices rendering onsite trace detection [1], [29]. Cellulose, due to its low cost, flexibility, and recyclability finds application in wide range of bio-detection techniques with ease contrary to conventional substrates [1], [28]. Paper-based sensors offer capillary action for rapid adhesion and sensor surface area to analyte molecules. Variety of techniques have been explored for the development of flexible paper-based SERS sensors, like printing, dipping, PVD, and SILAR to fabricate metal nanostructures onto paper requiring costly instruments, and multi-reaction steps [1], [22]–[32].

Herein, we report a cost-effective and simple in-situ silver mirror reaction (SMR) for the growth of silver-based plasmonic multifaceted nanostructures on the paper based plasmonic flexible substrate (PPFS) for SERS sensing. This technique provides multifaceted growth of Ag nanostructures on paper for SERS sensing of UA and LA and their mixtures. Further, the aM sensitivity of Rh-6G was achieved on PPFS SERS substrate. The applicability of this technique finds immense potential based on its cost of fabrication, availability, for the identification of various other analytes in detection and preventive healthcare systems.

II. Materials and Methods

A. Materials and Plasmonic Paper Fabrication

Silver nitrate ($AgNO_3$), D-glucose (dextrose), Rh-6G, uric acid, lactic acid, and Whatman filter paper (R 42) were purchased from Sigma Aldrich (India). Ammonia solution (28%) was procured from Fisher Scientific, and double-distilled water obtained from Millipore Milli-Q system (Millipore Corp., U.S.A) was used throughout the experiment. Petrie dish, and glass beakers were washed properly with HCl/HNO_3 solution/DI water. AgNS nanostructures were in-situ grown on Whattman filter paper (grade 42) through silver mirror reaction (SMR) [29]. Before initiating SMR process, surface of the paper was mechanically smoothened via roller press. In the first step, this paper was fixed at the bottom of petri-dish, afterwards 5 ml $AgNO_3$ (0.01 M) solution, and 3 ml of NH_3 solution was poured one by one on the paper. This, led to the formation of brown color silver oxide precipitate later an equal amount of NH_3 solution was added again to it, fostering subsequent removal of silver oxide. In the last step, 5 ml of D-glucose solution (2M) was added drop by drop to the above solution, and the petri-dish was heated to 80 °C for 12 min to complete the SMR process. Later, AgNS grown filter paper was taken out, cleaned by ethanol and water to remove excess deposited material, and dried in a vacuum oven for 24 hrs. at 45 °C. Similarly, various samples C1, C2, C3, C4, and C5 were developed using the varied concentration of silver nitrate from 0.01, 0.1, 0.2, 0.3, and 0.4 M utilizing the SMR process to study the effect of silver ion content in shaping the size of silver nanostructures.

B. PPFS Substrate Preparation and Measurement

AgNS grown PPFS were taken in pieces of 0.5×0.5 cm^2 and made to fix on a glass slide for SERS measurement. PPFS SERS substrate was validated by sensing of Rh-6G dye at different concentrations, (mM-aM) solution. A fixed quantity, 5 μl solution of Rh-6G was drop-casted on the substrate and dried completely for 12 hrs to evaluate the SERS activity. Similarly, varied samples of LA (mM-μM) and UA (mM-pM) were prepared on PPFS for SERS activity. Further, the selectivity experiment was performed by mixing UA and LA at different concentrations (UA + LA 10^{-3}M (M-2), UA + LA: 10^{-6}M (M-3), and UA (10^{-12}M)+ LA (10^{-6}M) (M-4)) and compared with 10^{-3}M of UA and LA spectra (M1 and M5). Moreover, prepared substrates were compared with the commercially purchased substrate (Standard), by Metrohm, India, Pvt. Ltd., for the detection of UA, LA and their mixtures. For SERS sensing substrate was divided into 10 segments, and from each segments Raman spectra were collected to evaluate the relative standard deviation (RSD) values.

C. Measurement Techniques

Surface morphology of as-grown Ag nanostructures on paper were investigated by ZEISS Gemini, Supra 40 VP, Field Emission scanning electron microscopy (FESEM). The XRD analysis (2θ = 5 -85°), by PANalytical X'pert Pro X-ray diffractometer (λ = 1.5416Å). FTIR of the AgNS grown on paper was evaluated from Agilent FTIR Nicolet. FEI Titan G2 80-300 keV TEM, was used for the detection of particle dimension. Raman spectroscopy of the sample for SERS was conducted on micro-Raman STR, AIRIX/Technos corporation,

(Princeton instruments Acton spectra Pro 2500i spectrometer attached) having 532 nm DPSS Laser (Quantum Gem 50 mW).

III. Results and Discussion

A. Plasmonic Paper Substrate (PPFS) Characterization

In-situ growth of silver nanostructures (AgNS) employing silver-mirror reaction (SMR) is well established technique to achieve AgNS on various substrates such as metallic sheets, polymers, and nanofibers [30]–[32]. However, SMR had not been explored much on flexible paper substrates. Therefore, here SMR was employed on filter paper-based substrate to achieve plasmonic nanostructures, owing to its unique features, like low cost, flexibility, and porosity. Also, it offers adsorption, and capillary process, through its pores to facilitate analyte capture and its confinement for SERS sensing [30]–[32]. Smoothening of paper leads to uniformity and homogeneity of paper substrate for AgNS development. Anchoring and adsorption of silver ions in the SMR process is favored via the natural available pores on paper. SMR is a redox reaction in which $[Ag(NH_3)_2]^+$ is reduced to AgNS via reaction with aldehyde (−CHO) groups of glucose [24]. Later step is highly facilitated by the attraction of $[Ag\ (NH_3)_2]^+$ to hydroxyl (OH^-) species available onto paper through electrostatic attraction in the presence of aldehyde (−CHO) groups to AgNS [29].

FTIR analysis was conducted to examine the organic groups associated with the bare paper, and in-situ grown silver nanostructures on paper samples (C2, C3), as shown in SI (Fig.S-1). The presence of FTIR peak at 3450 cm^{-1}, corresponds to −OH stretching of intramolecular hydrogen bonds, which being characteristic of cellulose paper [29], [30]. The transmission (%) of FTIR signal, decreases with increasing silver loading content which reflects the dense growth of silver nanostructures on paper, SI (Fig.S-1). Thus, FTIR results establish the presence of −OH functional group, that could bond with various possible analytes for its immobilization, and thus playing a key role in the SERS detection phenomenon.

To understand the effect of silver ion content on the growth of particle size and structural morphology of silver nanostructures used in the SMR process, various samples like C1 (0.01M), C2 (0.1M), C3 (0.2M), C4 (0.3M), and C5 (0.4M) were prepared by varying silver ion content. TEM images of all the samples C1 (0.01M), C2 (0.1M), C3 (0.2M), C4 (0.3M), and C5 (0.4M) have been shown in Fig. 1(a-e). The morphology of AgNS from Fig.1-a) (sample C1), is found to be spherical with an average size ∼50 nm, on the contrary morphology of AgNS in Fig.1-b) (sample C2) is deviated from spherical to triangular, hexagonal, and others with average size ∼72 nm. This trend of multifacet growth of AgNS continues to evolve from sample C2 onwards as observed in all samples viz., C3, C4, and C5 as evident from Fig. 1 (c-e).

Further, it could be established that the average particle size for samples C3, C4, and C5 (Fig. 1 (c-e)) is found to be ∼58, 162, and 220 nm respectively, which increases with the silver ion content in SMR. In summary, the increasing silver ion content (0.01, 0.1, 0.2, 0.3, 0.4M) in the SMR process leads to the growth of multifaceted silver structures along with the particle size of AgNS. Hence, the growth of multifaceted AgNS, and its dependency on the silver ion content used in the SMR process is concluded, thus facilitating PPFS for SERS application.

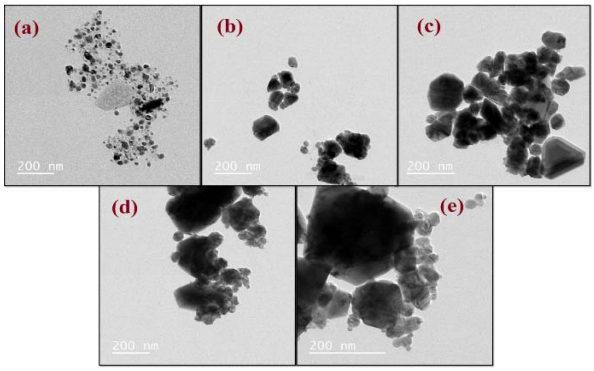

Fig. 1. (a-e) TEM images of Ag nanostructures synthesized at different silver ion content (0.01, 0.1, 0.2, 0.3, 0.4M) and its morphological (multifaceted) evolution, particle size variation.

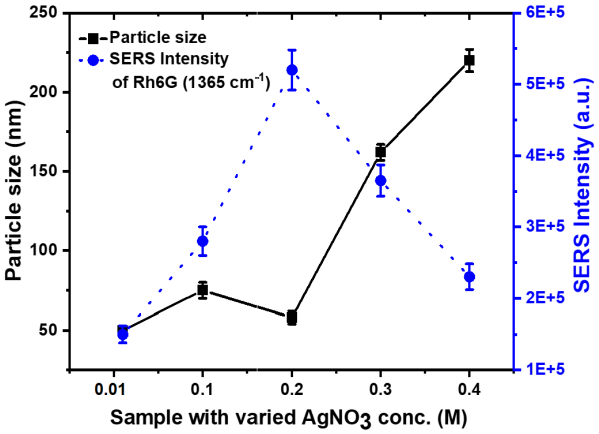

Fig. 2. Graph showing the effect of silver ion content on the size of silver nanostructures and the variation of SERS intensity of Rh-6G (mM) solution.

B. PPFS Substrate for SERS Application

SERS has facilitated the tracing down of dyes to a single-molecule regime due to its high signal enhancement [31]–[33]. The optimization studies of various PPFS substrates were undertaken by evaluating the SERS signal intensity of Rh-6G (1365 cm^{-1}) dye solution (mM) on various samples C1-C5. The variation of SERS intensity of 1365cm^{-1} peak of Rh-6G achieved on different substrates (C1-C5) has been plotted in Fig.2. It was found that the sample C3 (0.2M) of AgNS with size ∼58 nm exhibits the highest enhancement compared to its counterpart samples (C1, C2, C4, and C5). Thus, apart from the size of the AgNS, the surface morphology (facets) offers multiple scattering centers on single structure, promoting SERS signal enhancement [22]–[34].

The above trend of SERS intensity elucidates the decisive role of the size of silver nanostructures, apart from morphology (multifaceted pattern) of AgNS, in which previous supersedes the latter after C3 sample (∼58 nm).

SERS signal for sample C1 and C2 increases till C3, due to the evolution of multifaceted AgNS structure, later it decreases after C3, i.e., for C4 and C5 samples which is due to the

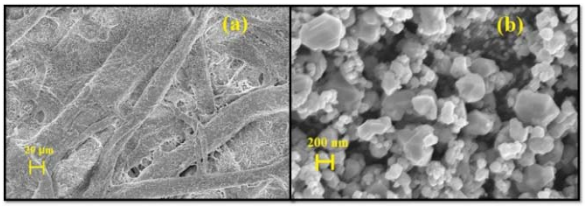

Fig. 3. FESEM images of AgNS growth on PPFS substrate, sample C3 (0.2 M) (a) fibrous nature of the substrate for confinement and capture of analyte (b) growth of multifaceted AgNS at 200 nm scale.

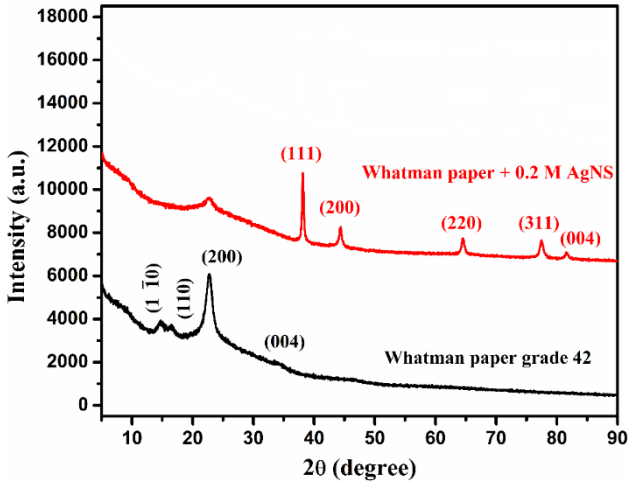

Fig. 4. XRD pattern of bare paper and in-situ grown silver nanostructures on PPFS by SMR process (0.2M silver content).

reduced no. of 'hot spots' resulting from large structures occupying the same area for SERS scattering. Hence, the optimized AgNS growth obtained at 0.2M (C3) silver ion content with an average particle size∼58 nm and having five-fold twinned icosahedron (discussed later in TEM section) was found to be best compared to its counterparts.

The optimized sample, C3 was further subjected to various studies like FESEM, XRD, and HRTEM to get better insights into the morphological, crystallographic, and particle size aspects of as-prepared silver nanostructures on paper by SMR.

The surface morphology, distribution, and homogeneity of silver nanostructures of as-synthesized samples C2 (0.1M), C3 (0.2M), C4 (0.3M) grown on PPFS substrates was evaluated from FESEM (Fig. S-2). FESEM images of C3, as shown in Fig.3-a) at 20μm scale reflect the fibrous nature substrate (paper), whereas, at high magnification of 200 nm, Fig.3-b) the highly dense growth of multifaceted AgNS nanostructures on paper could be confirmed.

Such morphology (multifaceted) and growth pattern (dense) could highly favor the SERS activity, via number of hot spots and multiple scattering centers residing on single nanostructures [32], [36]. Clustering of nanostructures is facilitated from the available natural pores and fibrous nature of filter paper which could range from μm to nm scale which favors the density-dependent pattern. A comparison of the sample C3 has been done with C2 and C4, shown in Fig. S-2.

Hence from the FESEM studies (Fig. S-2), the growth of dense multifaceted silver nanostructures on PPFS substrate is confirmed which also, supports the FTIR results of Fig.S-1.

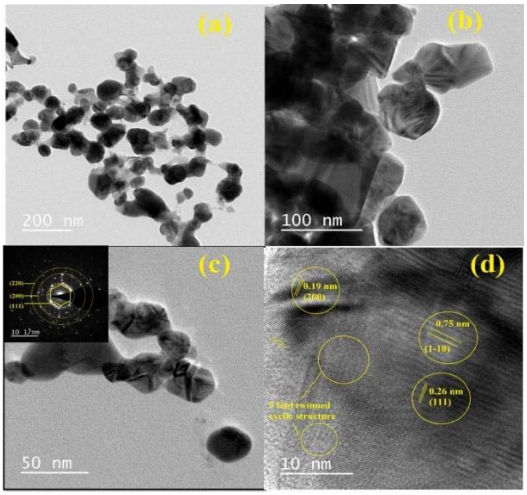

Fig. 5. (a) TEM image showing particle size distribution of silver nanostructures ∼58 nm (b) multifaceted AgNS on bare paper (c) few particles <50 nm with multifaceted morphology, and SAED pattern showing the various planes and the hexagonal (d) lattice planes observed.

To ascertain the crystal structure and lattice planes of AgNS fabricated on paper, its evaluation was conducted from XRD analysis. XRD pattern of the bare paper and in-situ grown silver nanostructures on paper are shown in Fig.4.

Diffraction planes (110), (110), (200), and (004) occurring at 2θ values of 14.73°, 16.68°, 22.68°, and 34.07°, represent the polycrystallinity due to cellulose (bare paper), similar trend is seen throughout all samples (C1, C2, C3) [24]–[27]. Since SMR leads to the growth of Ag nanostructures on paper, Ag planes (111), (200), (220), (311) and (004) at 2θ values of 38.12°, 44.34°, 64.54°, 77.44°, and 81.59° could also be seen. All these Ag diffraction planes are found to be consistent with JCPDS (file no: 89-3722) data of face-centered cubic (FCC) crystallography of Ag, with a = b = c = 4.111 Å. Hence the growth of silver nanostructures on the paper is confirmed from the above XRD analysis.

In the next stage, sample was subjected to TEM for particle size and SAED pattern analysis, as shown in Fig 5-c). which represents the multifaceted growth of AgNS having particle size distribution lying between 54-60 nm, Fig.5-a).

The growth of multifaceted silver nanostructure is established from Fig. 5 (b-c), these multifacets serve as multi-scattering centers located on single silver species for enhancing SERS signal intensity. Few multifaceted silver nanostructures (Fig.5-c) are found to be <50 nm, thus also the role of dimension, along with surface morphology could be expected to play important role in SERS signal enhancement. These multi-edge morphologies of silver are prominently found in Fig.2, and also supported from SAED pattern (inset Fig. 5-c) providing access of multi-edge scattering centres (multifaceted) to light for SPR enhancement. Fig. 5-d shows the lattice fringes supporting the cellulose (1-10), and planes of the silver (111), (200), also observed in the XRD pattern of the as-prepared sample.

Moreover, the appearance of a 5-fold twinned cyclic structure in Fig.5-d) also supports the multi-edge silver nanostructure as depicted from Fig.2 and Fig.5-b). Thus, the growth of multifaceted Ag nanostructures is confirmed from the above

analysis, which is expected to boost the SERS activity, via multi-plasmon scattering centers thereby offering high SERS signal intensity.

C. PPFS SERS Substrate Validation With Rhodamine-6G

Dyes find a prominent role in various applications from coloring, food, textiles, paper, and biological research. It provides the highest signal enhancement for Raman scattering due to resonances that contribute to Herzberg-Teller coupling; like surface plasmon resonance (SPR) contributed by plasmonic nanoparticles, the molecular resonance from dye molecule, and finally the charge transfer from plasmonic substrate to dye molecule [32]–[34]. In this section, the SERS activity of the paper-based substrate was evaluated from Rh-6G dye solution, drop-casted on the substrate in different concentrations (mM-aM) as shown in Fig.6-a). Various Raman peaks specific to Rh-6G (mM solution) were observed as shown in Fig.6-a), like at 620 and 780 cm^{-1} (xanthene ring deformations (XRD)), 1190 cm^{-1} (XRD, C-H, and N-H bend), 1320 cm^{-1} (xanthene ring breath (XRB), N-H bend, CH_2 wag), 1390 cm^{-1} (xanthene ring stretch (XRS), in-plane C-H bend), 1520 cm^{-1} (XRS, C-N stretch, C-H and N-H bend), 1570 cm^{-1} (XRS, in-plane N-H bend), 1650 cm^{-1} (XRS, in-plane C-H bend) [34]–[36]. Peak at 1390 and 1650 cm^{-1} were identified and traced to aM concentration of Rh-6G on plasmonic paper, as shown in Fig.6-a). Limit of detection (LOD) was calculated from equation (E1) as shown in SI. The plot of LOD for Rh-6G has been shown in Fig. 6-b), the plot depicts a LOD value of 4.54×10^{-18} M, with a high degree of the correlation coefficient (R^2) = 0.9969.

The growth of AgNS, on paper owes to its surface uniformity, and porosity which serves as natural sites, to capture and confinement of analyte molecules. Besides this the multi-faceted AgNS also facilitates edge scattering centers to surface plasmon, forming multi-exciton centers (hot spots), generating intense SERS signal.

D. Detection of Lactic and Uric Acid

In the next step detection of lactic acid (LA) was conducted at different concentrations (mM-μM) on the PPFS sensor, results are shown in Fig. 7-a). Raman peak of LA corresponding to 925 cm^{-1}(CH_3 vibrations), 1050 cm^{-1} (C-CH_3), 1085 cm^{-1} (CO), 1120 cm^{-1} (CH_3, CO), 1390 cm^{-1} (CH_3, OH), 1585-90 cm^{-1} (CH_3,) 1616 cm^{-1} (C = O) were recorded for mM solution as shown in Fig.7-a) [37]–[39]. These peaks were assigned as signature peaks for detecting presence of LA at different concentrations, which reflects a μM sensitivity of the plasmonic paper sensor (Fig 7-a).

LOD value of LA was achieved using equation E1, SI, from the linear region of the fitted curve, as shown in Fig. 7-b) which depicts a value of 0.56×10^{-6} M with R^2 = 0.9477 representing the high degree of homogeneity in the data points. Thus, a micromolar sensing capability of the paper-based sensor for LA was confirmed from the above analysis. Comparative details from the reported literature values, have been presented in SI (Table S1).

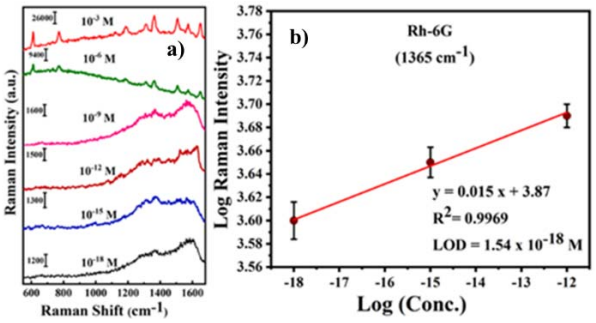

Fig. 6. SERS activity on PPFS substrate (a) Rh-6G detection (aM) of AgNS paper (b) LOD value calculated with R^2 = 0.9969 of 1.54×10^{-18} M.

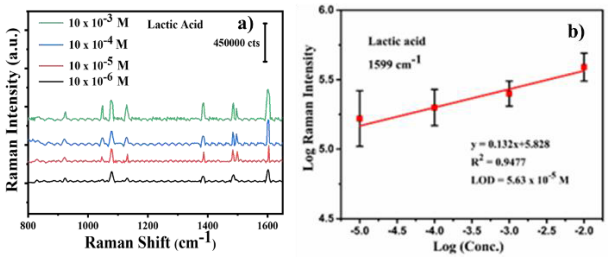

Fig. 7. SERS activity on PPFS substrate (a) for detection of LA at different concentration (mM- μM) (b) calculation of LOD value of 0.56×10^{-6} M with R^2 = 0.9477 from the linear plot.

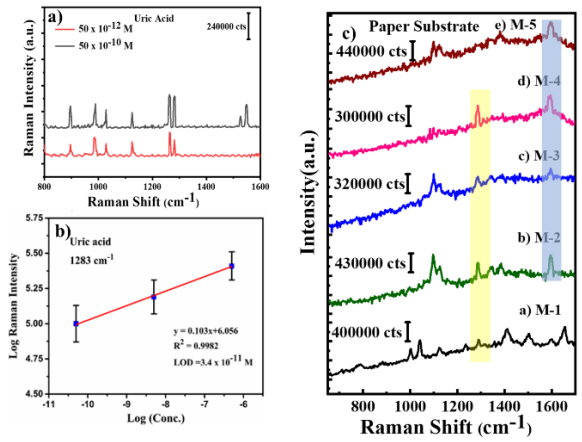

Fig. 8. (a) SERS spectra of UA at different concentrations (10^{-10}, 10^{-12}M), (b) Limit of detection (LOD) determination yields a value of 0.34×10^{-12} M with R^2 = 0.9982 and c) Selectivity spectra of LA and UA on C3.

Similarly, the detection of uric acid (UA) on the paper-based SERS sensor was conducted at different concentrations (10^{-10}-10^{-12}) as shown in Fig.8-a). The SERS spectra of UA from 10^{-3}M to 10^{-8}M is shown in Figure S-3. Various Raman bands could be detected at 875 cm^{-1} (N-H bending), 980 cm^{-1} and 1020 cm^{-1} (ring vibrations), 1120 cm^{-1} 6 1280 cm^{-1} (N-C-C stretching and bending), 1290 cm^{-1} and 1520 cm^{-1} (C-O and asymmetric NH_3) 1560 cm^{-1} (C-N vibrations) [39], [40]. The observation of these above Raman peaks down to pM level (Fig. 8-a) reflects the high sensitivity of the sensor for UA. Further, the LOD calculation was conducted from the fitted values shown in Fig.8-b), which shows a value of 0.3×10^{-12} M with R^2 = 0.9982. A comparison of the SERS technique employing various substrates, and their order of sensitivity/LODs have been shown in SI (Table S-1),

which depicts the sensor's ability and detection level. Thus, analysis of SI (Table S-1), shows that, this plasmonic paper demonstrates better detection level for Rh-6G, LA and UA than reported values on plasmonic-based paper substrates. The uniformity and reproducibility of PPFS SERS substrate were evaluated from the relative standard deviation (RSD) of Raman intensities, obtained from 10 different spots of each substrate of three different batches. RSD values of Rh-6G, LA, and UA was calculated using equation E2, S.I. The RSD values for Rh-6G, LA, and UA were found to be 3.52, 9.43, and 12.7%.

The calculation of average enhancement factor (EF) for the analytes were obtained by the equation (E3) as shown in SI. The EF for Rh-6G, LA, and UA was evaluated to 2.5×10^{15} and 6.6×10^{11}, 2.14×10^{4} values. Thus, these values of enhancement factor depict the high degree of sensitivity of SERS paper, along with ease of fabrication, and growth of multifaceted AgNS by SMR on PPFS sensor.

IV. Selectivity and Comparative Studies

Selectivity is a key parameter to evaluate performance of any SERS substrate. To demonstrate selectivity on PPFS substrate, UA, LA and their mixture solutions were prepared (M1, M2, M3, M4 and M5) and SERS spectra were recorded (Figure 8-c). Our results indicate that PPFS substrate can selectively detect UA and LA from their mixtures. Further, the performance of the PPFS substrate was tested with commercially available SERS substrate (Metrohm India, Pvt. Ltd.) for UA, LA and their mixtures respectively and shown in Figure S6, SI. The selectivity data of PPFS (Figure 8-c) and the commercially obtained substrate (Figure-S-4) was compared as shown in Figures S-5 (Note:S-5) and S-6 (Note:S-6), SI. Obtained results indicate that SERS intensity is better on the PPFS substrate individually (UA and LA) as well as in their mixtures as compared to the commercial standard substrate. Hence, the PPFS has a potential to be used as a highly sensitive and selective SERS substrate for practical applications.

V. Conclusion

In this work, facile growth of multifaceted AgNS on the PPFS substrate was achieved through SMR. Thereafter, the PPFS substrate were employed to detect Rh-6G, a dye molecule, LA and UA acid biomarkers for preventive healthcare. The PPFS SERS substrate demonstrated high sensitivity for Rh-6G dye with a LOD value of 1.54 aM. Sensitivity for LA and UA were evaluated to LODs of 0.6 μM and 0.3 pM levels. These SERS detection levels for UA are two orders better, whereas for LA it is superior to the reported literature findings for paper-based SERS sensors. Further, selectivity and comparison of the PPFS substrate experiments were done. It was found that the obtained SERS intensity is better on the PPFS substrate individually as well as in their mixtures for UA and LA as compared to the commercial substrate. Hence, the prepared paper substrate has a potential to be used as a highly sensitive and selective SERS substrate for practical applications. We attribute this sensitivity level of the sensor to the dense growth of multifaceted AgNS on PPFS, which provides multiple-sharp edges facilitating scattering of surface plasmon resonance for high SERS sensitivity.

Acknowledgment

The authors Prabhat K. Dwivedi and Manish M. Kulkarni thank Nano Mission, DST, New Delhi, for supporting the ongoing work at the Center for Nanosciences.

References

[1] K. Xu, R. Zhou, K. Takei, and M. Hong, "Toward flexible surface-enhanced Raman scattering (SERS) sensors for point-of-care diagnostics," *Adv. Sci.*, vol. 6, Jul. 2019, Art. no. 1900925.

[2] E. Sohn, "Diagnosis: Frontiers in blood testing," *Nature*, vol. 549, pp. S16–S18, Sep. 2017.

[3] S. Abalde-Cela *et al.*, "A SERS-based 3D nanobiosensor: Towards cell metabolite monitoring," *Mater. Adv.*, vol. 1, pp. 1613–1621, Sep. 2020.

[4] P.-H. Hsu and H. K. Chiang, "Surface-enhanced Raman spectroscopy for quantitative measurement of lactic acid at physiological concentration in human serum," *J. Raman Spectrosc.*, vol. 41, pp. 1610–1614, Dec. 2010.

[5] S. Kim *et al.*, "Quasi-3D plasmonic nanowell array for molecular enrichment and SERS-based detection," *Nanomaterials*, vol. 10, no. 5, p. 939, May 2020.

[6] Y. Hu *et al.*, "Surface enhanced Raman scattering active gold nanoparticles with enzyme-mimicking activities for measuring glucose and lactate in living tissues," *ACS Nano*, vol. 11, no. 6, pp. 5558–5566, May 2017.

[7] W. Zhang, C. Guo, K. Jiang, M. Ying, and X. Hu, "Quantification of lactate from various metabolic pathways and quantification issues of lactate isotopologues and isotopmers," *Sci. Rep.*, vol. 7, p. 8489, Aug. 2017.

[8] C. S Pundir, V. Narwal, and B. Batra, "Determination of lactic acid with special emphasis on biosensing methods: A review," *Biosensors Bioelectron.*, vol. 86, pp. 777–790, Dec. 2016.

[9] J. Seheult, G. Fitzpatrick, and G. Boran, "Lactic acidosis: An update," *Clin. Chem. Lab. Med.*, vol. 55, no. 3, pp. 322–333, Mar. 2017.

[10] P. Wang, X. Wang, Y. Sun, G. Gong, M. Fan, and L. He, "Rapid identification and quantification of the antibiotic susceptibility of lactic acid bacteria using surface enhanced Raman spectroscopy," *Anal. Methods*, vol. 12, pp. 376–382, Oct. 2020.

[11] R. K. Saravanan, T. K. Naqvi, S. Patil, P. K. Dwivedi, and S. Verma, "Purine-blended nanofiber woven flexible nanomats for SERS-based analyte detection," *Chem. Commun.*, vol. 56, pp. 5795–5798, Apr. 2020.

[12] C. Westley, Y. Xu, B. Thilaganathan, A. J. Carnell, N. J. Turner, and R. Goodacre, "Absolute quantification of uric acid in human urine using surface enhanced Raman scattering with the standard addition method," *Anal. Chem.*, vol. 89, no. 4, pp. 2472–2477, Jan. 2017.

[13] L. Zhao, J. Blackburn, and C. L. Brosseau, "Quantitative detection of uric acid by electrochemical-surface enhanced Raman spectroscopy using a multilayered Au/Ag substrate," *Anal. Chem.*, vol. 87, no. 1, pp. 441–447, Jan. 2015.

[14] J. E. L. Villa and R. J. Poppi, "A portable SERS method for the determination of uric acid using a paper-based substrate and multivariate curve resolution," *Analyst*, vol. 141, pp. 1966–1972, Jan. 2016.

[15] M. T. Alula, P. Lemmens, L. Bo, D. Wulferding, J. Yang, and H. Spende, "Preparation of silver nanoparticles coated ZnO/Fe_3O_4 composites using chemical reduction method for sensitive detection of uric acid via surface-enhanced Raman spectroscopy," *Anal. Chim. Acta*, vol. 1073, pp. 62–71, Sep. 2019.

[16] X. Guo *et al.*, "Method study on determination of total purine content in fish meat by diazotization reaction combined with SERS," *LWT*, vol. 123, Apr. 2020, Art. no. 109027.

[17] C.-Y. Huang and H.-C. Hsiao, "Integrated EC-SERS chip with uniform nanostructured EC-SERS active working electrode for rapid detection of uric acid," *Sensors*, vol. 20, no. 24, p. 7066, Dec. 2020.

[18] X. Liu *et al.*, "Large scale flexible surface enhanced Raman scattering (SERS) sensors with high stability and signal homogeneity," *ACS Appl. Mater. Interfaces*, vol. 12, no. 40, pp. 45332–45341, Sep. 2020.

[19] V. Moisoiu *et al.*, "Breast cancer diagnosis by surface-enhanced Raman scattering (SERS) of urine," *Appl. Sci.*, vol. 9, p. 806, Feb. 2019.

[20] A. Wang, C. Guan, G. Shan, Y. Chen, C. Wang, and Y. Liu, "A nanocomposite prepared from silver nanoparticles and carbon dots with peroxidase mimicking activity for colorimetric and SERS-based determination of uric acid," *Microchim. Acta*, vol. 186, p. 644, Aug. 2019.

[21] Z. Li, X. Huang, and G. Lu, "Recent developments of flexible and transparent SERS substrates," *J. Mater. Chem. C*, vol. 8, pp. 3956–3969, Mar. 2020.

[22] J. Xu, C. Cheng, S. Shang, W. Gao, P. Zeng, and S. Jiang, "Flexible, reusable SERS substrate derived from ZIF-67 by adjusting LUMO and HOMO and its application in identification of bacteria," *ACS Appl. Mater. Interfaces*, vol. 12, no. 44, pp. 49452–49463, Oct. 2020.

[23] Y. Bu *et al.*, "Bilayer composites consisting of gold nanorods and titanium dioxide as highly sensitive and self-cleaning SERS substrates," *Microchim. Acta*, vol. 184, pp. 2805–2813, Aug. 2017.

[24] G. Kwon, J. Kim, D. Kim, Y. Ko, Y. Yamauchi, and J. You, "Nanoporous cellulose paper-based SERS platform for multiplex detection of hazardous pesticides," *Cellulose*, vol. 26, pp. 4935–4944, Apr. 2019.

[25] H. Lim *et al.*, "A mesopore-stimulated electromagnetic near-field: Electrochemical synthesis of mesoporous copper films by micelle self-assembly," *J. Mater. Chem. A*, vol. 8, no. 40, pp. 21016–21025, 2020.

[26] S. A. Razek, A. B. Ayoub, and M. A. Swillam, "One step fabrication of highly absorptive and surface enhanced Raman scattering (SERS) silver nano-trees on silicon substrate," *Sci. Rep.*, vol. 9, p. 13588, Sep. 2019.

[27] H. Lim *et al.*, "Synthesis of uniformly sized mesoporous silver films and their SERS application," *J. Phys. Chem. C*, vol. 124, no. 43, pp. 2373–23730, 2020.

[28] V. T. N. Linh *et al.*, "A facile low-cost paper-based SERS substrate for label-free molecular detection," *Sens. Actuators B, Chem.*, vol. 291, pp. 369–377, Jul. 2019.

[29] B. Jiang *et al.*, "Morphology-controlled synthesis of silver nanoparticles on the silicon substrate by a facile silver mirror reaction," *AIP Adv.*, vol. 3, no. 3, Mar. 2013, Art. no. 032119.

[30] B. Duchemin, "Size, shape, orientation and crystallinity of cellulose I_β by X-ray powder diffraction using a free spreadsheet program," *Cellulose*, vol. 24, pp. 2727–2741, May 2017.

[31] S.-Y. Ding, E.-M. You, Z.-Q. Tian, and M. Moskovits, "Electromagnetic theories of surface-enhanced Raman spectroscopy," *Chem. Soc. Rev.*, vol. 46, pp. 4042–4076, Jun. 2017.

[32] K. L. Wustholz *et al.*, "Structure-activity relationships in gold nanoparticle dimers and trimers for surface-enhanced Raman spectroscopy," *J. Amer. Chem. Soc.*, vol. 132, no. 31, pp. 10903–10910, Jul. 2010.

[33] T. K. Naqvi *et al.*, "Hierarchical laser-patterned silver/graphene oxide hybrid SERS sensor for explosive detection," *ACS Omega*, vol. 4, no. 18, pp. 17701–17701, Oct. 2019.

[34] T. K. Naqvi, A. K. Srivastava, M. M. Kulkarni, A. M. Siddiqui, and P. K. Dwivedi, "Silver nanoparticles decorated reduced graphene oxide (rGO) SERS sensor for multiple analytes," *Appl. Surf. Sci.*, vol. 478, pp. 887–895, Jun. 2019.

[35] J. Wang, C. Qiu, X. Mu, H. Pang, X. Chen, and D. Liu, "Ultrasensitive SERS detection of rhodamine 6G and p-nitrophenol based on electrochemically roughened nano-Au film," *Talanta*, vol. 210, Apr. 2020, Art. no. 120631.

[36] K. Zhang, T. Zeng, X. Tan, W. Wu, Y. Tang, and H. Zhang, "A facile surface-enhanced Raman scattering (SERS) detection of rhodamine 6G and crystal violet using Au nanoparticle substrates," *Appl. Surf. Sci.*, vol. 347, pp. 569–573, Aug. 2015.

[37] C. Lux, A. Lubio, A. Ruediger, S. Robert, and C. Muehlethaler, "Optimizing the analysis of dyes by surface-enhanced Raman spectroscopy (SERS) using a conventional-microwave silver nanoparticles synthesis," *Forensic Chem.*, vol. 16, Dec. 2019, Art. no. 100186.

[38] X. Dong, R. Li, C. G. Schäfer, and F. Wang, "Composite MF@Ag-NPs microspheres for label-free quantitative detection of uric acid," *Colloids Surf. A, Physicochem. Eng. Aspects*, vol. 523, pp. 1–8, Jun. 2017.

[39] Y. Lu *et al.*, "Superhydrophobic silver film as a SERS substrate for the detection of uric acid and creatinine," *Biomed. Opt. Exp.*, vol. 9, no. 10, pp. 4989–4997, Oct. 2018.

[40] P.-H. Hsu, T.-H. Tsai, and H. K. Chiang, "*In vivo* blood lactic acid monitoring using microdialysis and surface-enhanced Raman spectroscopy," *Proc. SPIE, Int. Soc. Opt. Eng.*, vol. 7040, Sep. 2008, Art. no. 70400R.